IEEE Access
Multidisciplinary | Rapid Review | Open Access Journal

Received 31 May 2023, accepted 1 July 2023, date of publication 7 July 2023, date of current version 13 July 2023.

Digital Object Identifier 10.1109/ACCESS.2023.3293017

RESEARCH ARTICLE

Analysis of Transmission Characteristics of ECPT System Based on LCLC-LC Compensation

XIN GENG AND JIE XU
School of Electrical and Electronic Engineering, Harbin University of Science and Technology, Harbin 150080, China
Corresponding author: Xin Geng (6883892@qq.com)

ABSTRACT Based on the parameter design of the bilateral LC-type capacitively coupled wireless power transmission system, the T-type LCL impedance network is added to adjust the system voltage gain by adjusting the inductance value in the LCL network at the primary side. The numerical relationship and phase relationship between the output voltage and the input voltage in the resonant state are theoretically derived, and the corresponding mathematical expressions and the calculation expressions of the key parameters of the system are given. Finally, the feasibility and effectiveness of the proposed capacitively coupled wireless power transmission system and its parameter design method are verified by simulation and experiment.

INDEX TERMS Capacitance coupling, resonant network, impedance matching, wireless power transfer.

I. INTRODUCTION

For wet, hot, cold, underwater, mine, oil depot and other special working environment occasions, the traditional cable power supply method has great potential safety hazards. On the one hand, this kind of special environment often aggravates the aging of the line and the wear of the joint. On the other hand, the flexibility and waterproofness of the equipment are also greatly limited by the wired power supply method. Wireless Power Transmission (WPT) technology can effectively avoid many drawbacks caused by traditional power supply methods and achieve electrical isolation to a certain extent. The wireless power transmission technology comprehensively applies modern power electronic energy conversion technology, circuit theory, electromagnetic field theory, microelectronics technology and modern control theory to realize the transmission of electric energy through soft media (such as electric field, magnetic field, microwave, laser, etc.) in a non-electrical contact manner. At present, there are many research results based on Magnetic-field Coupled Wireless Power Transfer (MC-WPT) and Electric-field Coupled Power Transfer (ECPT), and the wireless power transfer technology based on magnetic field coupling is the most mature. It has been applied in rail transit [1], [2], consumer electronics [3], [4], [5], [6], [7], implantable medical [8], [9], [10], [11] and other fields. Compared with magnetic field coupling, the difference between electric field coupling wireless power transmission and magnetic field coupling is mainly in the coupling mechanism. In the research of compensation network, the difference between the two is not large. The outstanding advantages of electric field coupling mechanism are simple and thin, low cost, good shape plasticity of coupling mechanism, no eddy current loss. When working, the electric field energy is mainly concentrated between the coupling plates, which has little influence on the electromagnetic interference of the surrounding environment. It has a very broad application prospect in some power consumption fields with special requirements.

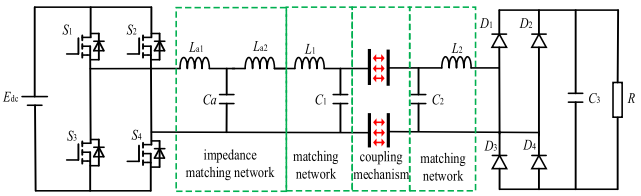

FIGURE 1. LCLC-LC compensation ECPT system topology diagram.

Figure 1 is the schematic diagram of the LCLC-LC compensated ECPT system topology proposed in this paper. The DC power supply is converted into a high-frequency AC output through a high-frequency inverter circuit, and a

The associate editor coordinating the review of this manuscript and approving it for publication was Razi Iqbal.

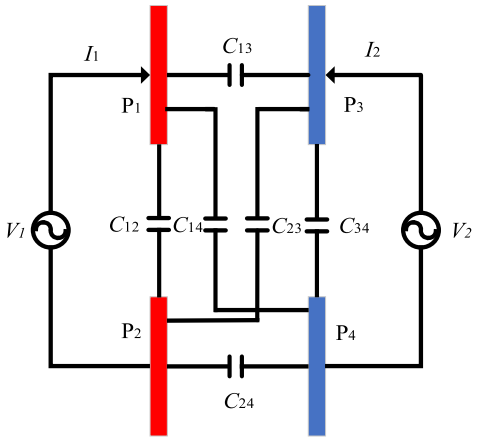

FIGURE 2. Quadrupole plate structure and capacitance model.

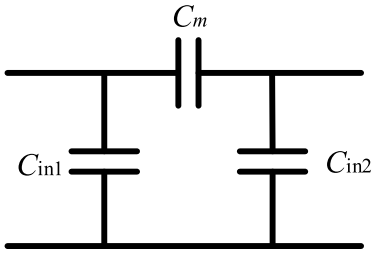

FIGURE 3. 3 Capacitor structure.

TABLE 1. Equivalent capacitance.

equivalent capacitance	C_m	C_{in1}	C_{in2}
value	250p	3.0865p	3.0552p

higher voltage is obtained after the T-type LCL impedance transformation network. After passing through the LC resonant network, it is transmitted to the coupling plate. The high-frequency electric field on the coupling plate generates a displacement current between the transmitting plate and the receiving plate. The displacement current is supplied to the rectifier bridge circuit after passing through the reverse LC resonant network, Thus, the wireless power transmission from the transmitter to the receiver is realized.

II. MODELING OF COUPLED MECHANISM

A. CAPACITANCE MODEL

Compared with the traditional magnetic field coupling system, the analysis of the coupling mechanism of the ECPT system is relatively complex. In the case of the coupling mechanism offset, the stray capacitance formed by the coupling mechanism and the surrounding objects will increase the proportion of the influence on the system. In this paper, the simple and widely used parallel quadrupole plate structure is adopted. ignoring the stray capacitance of the coupling plate and the surrounding environment, the four-stage plate structure and the capacitance model are shown in Figure 2:

Taking the P4 plate as the reference node, the voltage of V_1 and V_2 can be expressed as:

$$\begin{cases} V_1 = V_{P1} - V_{P2} \\ V_2 = V_{P3} \end{cases} \tag{1}$$

According to the capacitance model shown in Figure 2, the node voltage equation is written:

$$\begin{cases} I_1 = V_{P1}(j\omega C_{12} + j\omega C_{14} + j\omega C_{13}) - V_{P2}j\omega C_{12} \\ \qquad -V_{P3}j\omega C_{13} \\ -I_1 = V_{P2}(j\omega C_{12} + j\omega C_{23} + j\omega C_{24}) - V_{P1}j\omega C_{12} \\ \qquad -V_{P3}j\omega C_{23} \\ I_2 = V_{P3}(j\omega C_{13} + j\omega C_{23} + j\omega C_{34}) - V_{P1}j\omega C_{13} \\ \qquad -V_{P2}j\omega C_{23} \\ -I_2 = -V_{P2}j\omega C_{24} - V_{P3}j\omega C_{34} \end{cases} \tag{2}$$

Equations (1) and (2) combined with circuit transformation, V_1 and V_2 can be expressed as:

$$\begin{cases} V_1 = \dfrac{I_1}{j\omega C_{in1}} + V_2\dfrac{C_m}{C_{in2}} \\ V_2 = \dfrac{I_2}{j\omega C_{in1}} + V_1\dfrac{C_m}{C_{in2}} \end{cases} \tag{3}$$

The capacitance model shown in Figure 2 can be further equivalent to a three-capacitor structure:

Where Cm, Cin1, Cin2 can be expressed as:

$$\begin{cases} C_m = \dfrac{C_{24}C_{13} - C_{14}C_{23}}{C_{13} + C_{24} + C_{14} + C_{23}} \\ C_{in1} = \dfrac{(C_{13} + C_{14})(C_{23} + C_{24})}{C_{13} + C_{14} + C_{24} + C_{23}} + C_{12} - C_m \\ C_{in2} = \dfrac{(C_{13} + C_{14})(C_{23} + C_{24})}{C_{13} + C_{14} + C_{24} + C_{23}} + C_{34} - C_m \end{cases} \tag{4}$$

The size of the coupling plate can be arbitrarily determined according to the actual application requirements. This paper considers the influence of self-capacitance and cross-coupling capacitance, that is, the equivalent circuit model shown in Figure.3. Taking a square copper plate with a side length of 200 mm and a thickness of 1.8 mm and a transmission distance of 4 mm as an example, the parameters are designed. Based on the geometric parameters of the plate, the finite element simulation in Maxwell software is used, and the equivalent capacitance value is obtained according to (4), as shown in Table 1:

B. COUPLING MECHANISM CURRENT ANALYSIS

Figure 4 is the current diagram flowing through the coupling mechanism. The input current is mainly divided into two parts, one is the output current flowing like the receiving plate, and the other is the leakage current flowing into the surrounding environment.

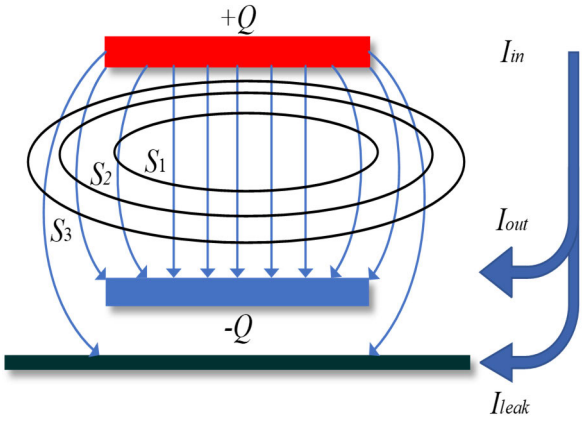

FIGURE 4. Current diagram of coupling mechanism.

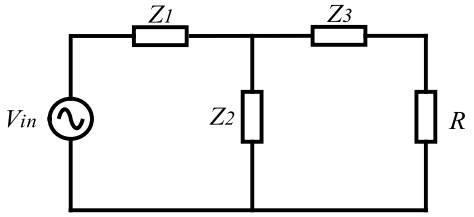

FIGURE 5. T-type network diagram.

The expressions of input current, output current and leakage current can be derived from Maxwell 's equations:

$$\begin{cases} I_{in} = \dfrac{d\vec{D}}{dt}S_3 = \varepsilon\dfrac{d\vec{E}}{dt}S_3 \\ I_{out} = \dfrac{d\vec{D}}{dt}S_1 = \varepsilon\dfrac{d\vec{E}}{dt}S_1 \\ I_{leak} = \varepsilon\dfrac{d\vec{E}}{dt}(S_3 - S_1) \end{cases} \tag{5}$$

I_{in} is the input current, I_{out} is the output current, I_{leak} is the leakage current, S_1, S_2 and S_3 are the size of the area containing the electric field line. (5) indicates the decisive factor of the coupling mechanism to flow through the current. When the coupling mechanism is loosely coupled, that is, when the transmission distance is large, a large part of the electric field line is coupled with the surrounding environment, thereby forming a leakage current, which affects the transmission efficiency of the entire system. In order to facilitate analysis, this paper is set to a tightly coupled state, the S_3 area is similar to the S_1 area, so that the input current is approximately equal to the output current, and the leakage current is 0.

III. IMPEDANCE MATCHING NETWORK AND RESONANT NETWORK ANALYSIS

A. ANALYSIS OF T-TYPE IMPEDANCE MATCHING NETWORK

The T-type impedance matching network belongs to the third-order network and consists of three energy storage components, as shown in Figure 5:

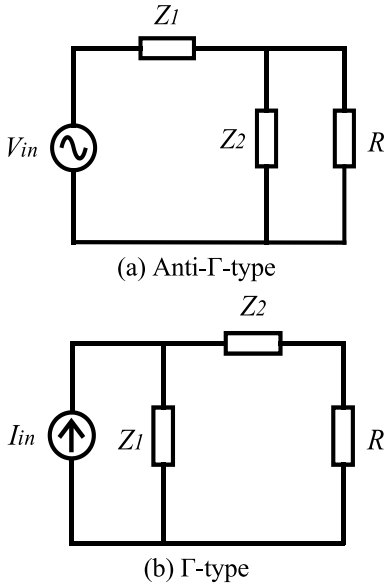

FIGURE 6. Second-order resonant network.

TABLE 2. Output characteristics of second-order resonant network.

Resonant network structure	Resonance conditions	Output
Γ-type resonant network	$Z_1 + Z_2 = 0$	$V_{out} = I_{in}Z_1$
Anti-Γ resonant network	$Z_1 + Z_2 = 0$	$I_{out} = \dfrac{V_{in}}{Z_1}$

By solving the mesh current equation for the T-type network, the output current and output voltage expressions can be obtained respectively:

$$\begin{cases} I_{T-out} = \dfrac{V_{in}Z_2}{(Z_2 + Z_3 + R)(Z_1 + Z_2) - Z_2^2} \\ V_{T-out} = \dfrac{V_{in}Z_2R}{Z_1Z_2 + Z_1Z_3 + Z_2Z_3 + (Z_1 + Z_2)R} \end{cases} \tag{6}$$

When the condition $Z_1Z_2 + Z_1Z_3 + Z_2Z_3 = 0$ is satisfied, the output voltage is independent of the load. the T-type network has an impedance transformation effect, and the output voltage can be expressed:

$$V_{out} = \frac{V_{in}Z_2}{(Z_1 + Z_2)} \tag{7}$$

B. SECOND-ORDER RESONANT NETWORK ANALYSIS

The second-order resonant network mainly has Γ-type and anti-Γ-type structures according to the structural form, as shown in Figure 6. There are only two energy storage elements, so the circuit relationship is simple. When the two energy storage elements satisfy the resonance condition, a certain output characteristic can be realized. Table 2 shows the output characteristics of the second-order resonant network.

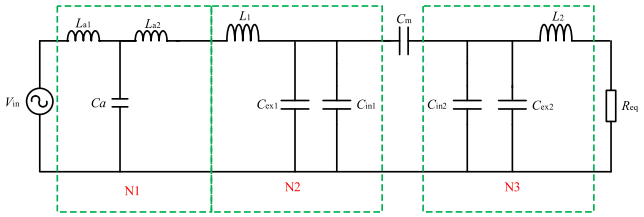

FIGURE 7. Equivalent circuit of ECPT system.

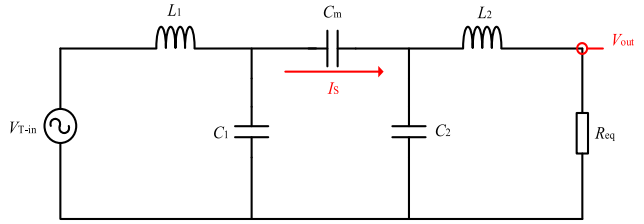

FIGURE 8. System simplified circuit.

IV. CHARACTERISTIC ANALYSIS AND PARAMETER DESIGN OF ECPT SYSTEM

Figure 7 is the equivalent circuit of the ECPT system. The inverter output is equivalent to the sinusoidal voltage source U_{in} by the fundamental wave approximation method. R_{eq} is the AC equivalent load, and the relationship with the load is $R_{\text{eq}} = 8R_{\text{L}}/\pi^2$. The coupling mechanism is equivalent to a 3-capacitor structure. The entire ECPT system is mainly composed of N1, N2, and N3 three networks. The N1 network is a T-type impedance matching network with a boost effect. The N2 network converts the output voltage of the T-type network into a constant current source, and the N3 is a Γ-type resonant network, which converts the constant current through the coupling mechanism into a constant voltage supply load.

Combine capacitance C_{ex1}, C_{in1} as C_1, Combine capacitance C_{ex2}, C_{in2} as C_2. When $Z_1Z_2 + Z_1Z_3 + Z_2Z_3 = 0$ is satisfied, V_{in} and T-network can be equivalent to $V_{\text{T-in}}$. $Z_1Z_2+Z_1Z_3+Z_2Z_3 = 0$ can be simplified to (8),The relationship between V_{in} and $V_{\text{T-in}}$ is shown in (9). The equivalent circuit of Figure 7 can be further simplified to the structure shown in Figure.8.

$$\omega^2 C_a \frac{L_{a1}L_{a2}}{L_{a1}+L_{a2}} = 1 \tag{8}$$

$$V_{T-in} = \frac{V_{in}}{(1-\omega^2 L_{a1}C_a)} \tag{9}$$

The parasitic resistance on the resonant inductor is not considered. From the analysis of the second-order resonant topology, it can be seen that under the resonant condition, the current flowing through the coupling capacitor C_{m} is approximately a constant current source. After passing through the Γ-type resonant network, the output voltage obtained on the load is approximately constant voltage, (10) is the system simplified circuit resonance condition, (11) is the current expression of the system flowing through the capacitor C_{m} under the resonance condition, (12) is the system output voltage expression.

$$\omega^2 L_1 C_1 = \omega^2 L_2 C_2 = 1 \tag{10}$$

$$I_S = \frac{V_{T-in}}{j\omega L_1} \tag{11}$$

$$V_{out} = -\frac{V_{T-in}}{\omega^2 L_1 C_2} \tag{12}$$

Let the ratio of the resonant capacitor C_2 to C_1 be β. According to the resonant condition (10), (12) can be further simplified:

$$V_{out} = -\frac{V_{T-in}}{\beta} \tag{13}$$

Substituting (9) into (13), the mathematical expressions of input voltage and output voltage are finally obtained under the conditions of Equations (8) and (10):

$$V_{out} = \frac{V_{in}}{-\beta(1-\omega^2 L_{a1}C_a)} \tag{14}$$

Because the resonant frequencies of the two sides of the coupling mechanism are the same, the values of L_1, L_2 and C_2 can be determined according to the resonant frequency condition and the capacitance ratio when the appropriate capacitance C_1 value is selected. In order to facilitate the analysis, the value of β is set to 1. Under the same resonant frequency, the T-type impedance network and the second-order resonant network can be designed independently. The voltage gain of the ECPT system is designed to be 5, the output voltage is in phase with the input voltage, and the operating frequency is set to be 600k. In the case of selecting the appropriate capacitance C_{a}, the parameters of L_{a1} and L_{a2} can be determined according to the equations (8) and (14). The system parameters designed in this paper are shown in Table 3:

TABLE 3. System parameters.

PARAMETER	VALUE	PARAMETER	VALUE
E_{dc}	1V	C_{ex1}	1200pF
f	600k	C_{ex2}	1200pF
C_{in1}	3.0865pF	L_1	58.4845uH
C_{in2}	3.0552pF	L_2	58.4845uH
L_{a1}	55.676uH	L_{a2}	281.1uH
C_{a}	1500pF	R	60

V. SIMULATION AND EXPERIMENTAL VERIFICATION

In order to verify the correctness of the parameter design method of the proposed ECPT system, the simulation model is established according to the parameters in Table 3. The inverter circuit structure adopts a full-bridge inverter structure, and the voltage amplitude is 1V. The simulation waveforms in Figure 9 are the input voltage waveform and the output voltage waveform of the T-type impedance matching network, the input voltage waveform and the output voltage waveform, the output voltage waveform and the output voltage waveform of the T-type impedance matching network, and the waveform between the input voltage and the input current.

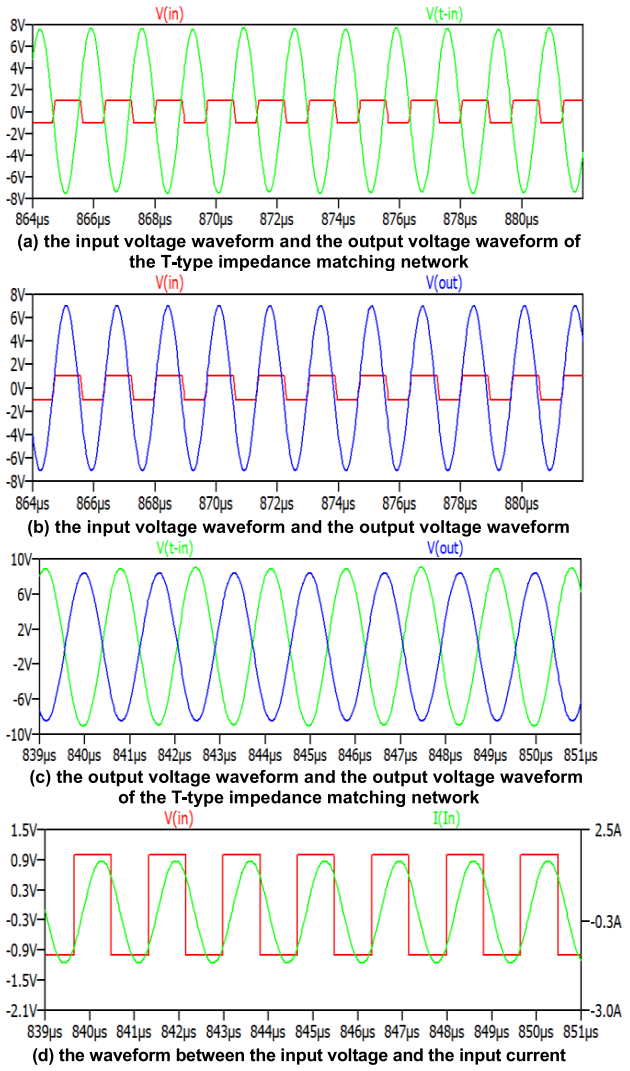

FIGURE 9. Simulation waves.

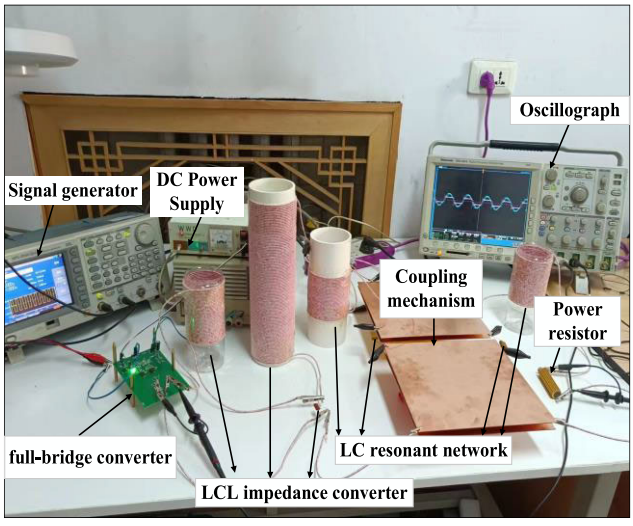

FIGURE 10. Experimental platform.

Since the β value is set to 1, according to (13), the output voltage $V_{\mathrm{T-in}}$ of the T-type network should be equal to the output voltage V_{out}, and the phase is reversed. Figure 9(c) shows that the output voltage amplitude is slightly lower than the output voltage $V_{\mathrm{T-in}}$ of the T-type network, but the phase is reversed, which is consistent with the theoretical derivation. According to the system parameter design in Table 3, the system voltage gain is 5, and the input voltage is in phase with the output voltage. Therefore, the phase of the input voltage is opposite to the output voltage of the T-type network. After the two-sided LC network is reversed, the input voltage and the output voltage are in phase. The correctness of the parameter design is verified in waveforms Figure 9 (a) and Figure 9 (b). Figure 9 (d) shows the input voltage waveform and the input current waveform. The input current waveform lags slightly behind the input voltage waveform, which is beneficial to realize the soft switching of the system to reduce the loss of the switch tube generated by the high frequency inverter circuit.

Figure 10 is the experimental device built in this paper, which mainly includes 8 parts: signal generator, DC power supply, inverter circuit, T-type network, primary side and secondary side LC network, coupling mechanism, power load and oscilloscope.

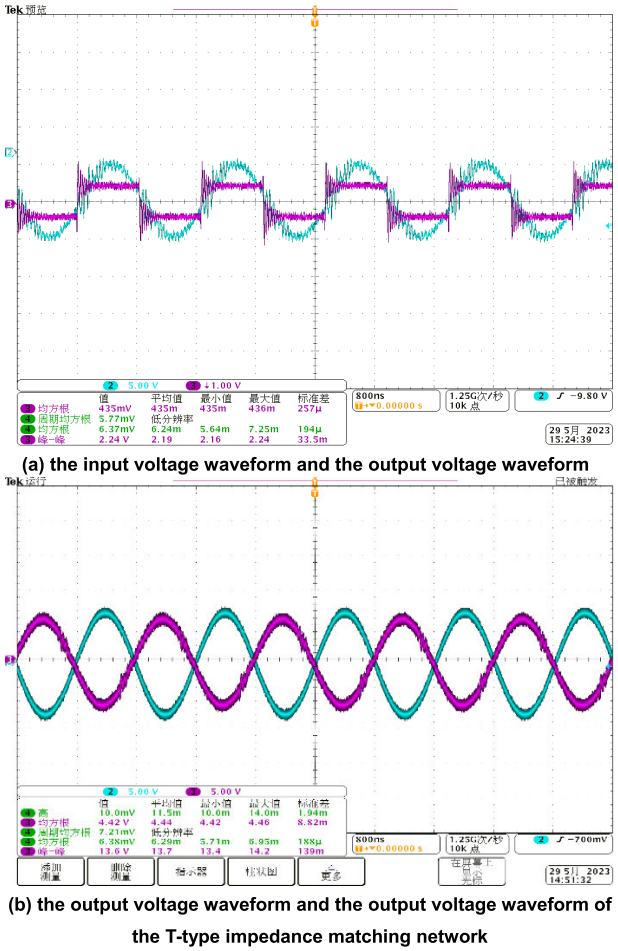

FIGURE 11. Experimental waveforms.

To reduce the loss of the system due to the skin effect, the inductance is wound by a high frequency Leeds wire of 0.1 mm $*$ 200. C_{ex1} and C_{ex2} capacitors use silver mica capacitors, and C_a uses polyethylene film capacitors, withstand voltage 1000 V. Due to the high operating frequency of the system, the general switching devices will have high switching losses. In this paper, the TI half-bridge power stage chip LMG5200 is used, which integrates two gallium nitride switches and drivers, which can greatly reduce external interference. Load resistance is power resistance. Figure 11 (a) and Figure 11(b) are the input and output waveforms and the output voltage waveform and output voltage waveform of the T-type impedance matching network.

Due to the error of inductance and capacitance, the measured waveform is slightly different from the simulated waveform. In addition, due to the influence of parasitic resistance on the inductor coil, the experimental voltage waveform value is slightly lower than the simulated waveform data, but it is generally consistent with Figure.10 (b) (c). Simulation and experiment show that the ECPT system parameter design is effective and accurate.

VI. CONCLUSION

Based on the parameter design of the bilateral LC-type ECPT system, this paper adds a T-type LCL impedance network to realize the voltage gain adjustment of the ECPT system by adjusting the inductance value of the LCL network on the primary side without changing the operating frequency of the system. The numerical relationship and phase relationship between input voltage and output voltage are deduced in detail, and the theoretical expression is given. Through the theoretical expression, the parameter design of ECPT system can be realized quickly, which simplifies the system design process.

In the theoretical analysis, the influence of inductance parasitic resistance on the system is not considered, which leads to the experimental waveform slightly lower than the simulation waveform. In the later research work, the influence of parasitic parameters in inductance and capacitance on the system will be studied, to realize the optimization of system parameters.

REFERENCES

[1] J. Dai and D. C. Ludois, "Wireless electric vehicle charging via capacitive power transfer through a conformal bumper," in *Proc. IEEE Appl. Power Electron. Conf. Expo. (APEC)*, Charlotte, NC, USA, Mar. 2015, pp. 3307–3313.

[2] J. Dai and D. C. Ludois, "Capacitive power transfer through a conformal bumper for electric vehicle charging," *IEEE J. Emerg. Sel. Topics Power Electron.*, vol. 4, no. 3, pp. 1015–1025, Sep. 2016.

[3] B. H. Choi, D. T. Nguyen, S. J. Yoo, J. H. Kim, and C. T. Rim, "A novel source-side monitored capacitive power transfer system for contactless mobile charger using class-E converter," in *Proc. IEEE 79th Veh. Technol. Conf. (VTC Spring)*, Seoul, South Korea, May 2014, pp. 1–5.

[4] J. Zhu, Y. Ban, R. Xu, and C. C. Mi, "An NFC-CPT-combined coupler with series-none compensation for metal-cover smartphone applications," *IEEE J. Emerg. Sel. Topics Power Electron.*, vol. 9, no. 3, pp. 3758–3769, Jun. 2021.

[5] K. S. Keerthi., K. Ilango., and G. N. Manjula., "Study of midfield wireless power transfer for implantable medical devices," in *Proc. 2nd Int. Conf. Biomed. Eng. (IBIOMED)*, Bali, Indonesia, Jul. 2018, pp. 44–47.

[6] S. Jeong, J. Jung, K. A. Kim, and J. Kim, "Analytical investigation of optimal wireless power transfer topology for electric vehicles," in *Proc. IEEE PELS Workshop Emerg. Technol., Wireless Power (WoW)*, Daejeon, South Korea, Jun. 2015, pp. 1–5, doi: 10.1109/WoW.2015.7132836.

[7] M. Wagih, A. Komolafe, I. Ullah, A. S. Weddell, and S. Beeby, "A wearable all-printed textile-based 6.78 MHz 15 W-output wireless power transfer system and its screen-printed Joule heater application," *IEEE Trans. Ind. Electron.*, early access, May 22, 2023, doi: 10.1109/TIE.2023.3277112.

[8] R. Jegadeesan, Y. X. Guo, and M. Je, "Electric near-field coupling for wireless power transfer in biomedical applications," in *Proc. IEEE MTT-S Int. Microw. Workshop Ser. RF Wireless Technol. Biomed. Healthcare Appl. (IMWS-BIO)*, Singapore, Dec. 2013, pp. 1–3.

[9] Y. Su, S. Xie, A. P. Hu, C. Tang, W. Zhou, and L. Huang, "Capacitive power transfer system with a mixed-resonant topology for constant-current multiple-pickup applications," *IEEE Trans. Power Electron.*, vol. 32, no. 11, pp. 8778–8786, Nov. 2017.

[10] M. A. Alomar, "Wavelet transform and cascaded feed forward neural network analysis of electromyographic data for involuntary detection of hand gesticulation," in *Proc. 1st Int. Conf. Innov. High Speed Commun. Signal Process. (IHCSP)*, Bhopal, India, Mar. 2023, pp. 402–406, doi: 10.1109/IHCSP56702.2023.10127203.

[11] F. Del Bono, A. Bontempi, A. Dentis, N. Di Trani, D. Demarchi, A. Grattoni, and P. M. Ros, "Design of a closed-loop wireless power transfer system for an implantable drug delivery device," *IEEE Sensors J.*, early access, May 3, 2023, doi: 10.1109/JSEN.2023.3270521.